

# Resonant inelastic x-ray scattering spectra in the hyperhoneycomb iridate $\beta$ -Li<sub>2</sub>IrO<sub>3</sub>: First principles calculations

V.N. Antonov,<sup>1,2</sup> D.A. Kukusta,<sup>1,3</sup> L. Uba,<sup>2</sup> A. Bonda,<sup>2</sup> and S. Uba<sup>2</sup>

<sup>1</sup>*G. V. Kurdyumov Institute for Metal Physics of the N.A.S. of Ukraine,  
36 Academician Vernadsky Boulevard, UA-03142 Kyiv, Ukraine*

<sup>2</sup>*Faculty of Physics, University of Białystok, K. Ciołkowskiego 1L, PL-15-245 Białystok, Poland*

<sup>3</sup>*Max-Planck-Institut für Festkörperforschung, Heisenberg Strasse 1, D-70569 Stuttgart, Germany*  
(Dated: January 18, 2021)

We studied the electronic structure of  $\beta$ -Li<sub>2</sub>IrO<sub>3</sub> insulator within the density-functional theory using the generalized gradient approximation with taking into account strong Coulomb correlations in the framework of the fully relativistic spin-polarized Dirac linear muffin-tin orbital band-structure method. The  $\beta$ -Li<sub>2</sub>IrO<sub>3</sub> undergoes a pressure-induced structural and magnetic phase transitions at  $P_c \sim 4$  GPa with symmetry lowering to the monoclinic  $C2/c$ . The structural phase transition is accompanied by the formation of Ir<sub>2</sub> dimers on the zigzag chains, with an Ir-Ir distance of  $\sim 2.66$  Å, even shorter than that of metallic Ir. The strong dimerization stabilizes the bonding molecular-orbital state, leads to the collapse of the magnetism and opens the energy gap with a concomitant electronic phase transition from a Mott insulator to band insulator. The resonant inelastic x-ray scattering spectra (RIXS) at the Ir  $L_3$  edge were investigated theoretically from first principles. The calculated results are in good agreement with the experimental data. We show that the drastic reconstruction of the RIXS spectral peak at 0.7 eV associated with the structural  $Fddd \rightarrow C2/c$  phase transition at  $P_c$  can be related to disappearing of the Coulomb correlations in the high-pressure  $C2/c$  phase.

PACS numbers: 75.50.Cc, 71.20.Lp, 71.15.Rf

## I. INTRODUCTION

Quantum spin liquids (QSLs) [1–3] represent a novel state of matter in which quantum fluctuations prevent the conventional magnetic order from being established, and the spins remain disordered even at zero temperature. It is an emerging and fast growing field. In this context the Kitaev Hamiltonian (KH) on honeycomb lattices has great promise [4]. The paramount attention given to such states can be understood by the fact that they may be topologically protected from decoherence [5], display fractional excitations with Majorana statistics, and therefore hold promise in the field of quantum information and quantum computation [6, 7]. The field of QSLs is still wide open, both theoretically and experimentally. So far, there have been a new experimental discoveries and theoretical ideas are rapidly emerging. However, a basic mathematical framework that can be used to understand QSLs systematically is still lacking. The major difficulty in understanding QSLs is that they are intrinsically strongly correlated systems, for which no perturbative approach is available.

Possible realization of such an exotic state has been suggested in Mott insulators such as 213 iridates A<sub>2</sub>IrO<sub>3</sub> (with A = Na, Li), which have a honeycomb layered structure consisting of IrO<sub>6</sub> octahedra [6, 8]. They have drawn much attention as a candidate for topological insulators [9, 10] with electron correlations. Both nontrivial hopping terms induced by the strong spin orbit (SO) coupling and significant on-site Coulomb correlations make honeycomb iridates a possible candidate also for the compounds with Kitaev spin liquid type ground state [11–17].

It was proposed that strong SO interaction in these iridates reorganizes the crystal field states of the  $5d$  orbitals into a  $J$ -multiplet structure, where  $J$  is the combined spin and effective orbital angular momentum. In this case, the Ir  $t_{2g}$  bands are most naturally described by relativistic atomic orbitals with the effective total angular momentum,  $J_{\text{eff}}=3/2$  and  $J_{\text{eff}}=1/2$ . In this approximation, the splitting between the  $3/2$  and  $1/2$  states is larger than their dispersion. The  $J_{\text{eff}}=1/2$  band is half-filled and the relatively weak Coulomb repulsion  $U$  is sufficient to split the  $J_{\text{eff}} = 1/2$  doublet into lower and upper Hubbard bands, giving rise to a novel Mott insulator [18].

There are several recent publications on the experimental and theoretical investigations of the electronic structure and various physical properties of honeycomb iridate Li<sub>2</sub>IrO<sub>3</sub> [13, 19–26]. However, the long-sought spin-liquid state has remained elusive. All three honeycomb polytypes of Li<sub>2</sub>IrO<sub>3</sub> (including  $\alpha$ ,  $\beta$ , and  $\gamma$  phases) are magnetically ordered that suggests that the Heisenberg interaction is still sizable. In addition, trigonal crystal fields also compete with the Kitaev interaction.

In the present study, we focus our attention on the theoretical investigation of the resonant inelastic x-ray scattering (RIXS) spectra in the  $\beta$ -Li<sub>2</sub>IrO<sub>3</sub> compound from first principles. RIXS is a fast developing experimental technique in which one scatters x-ray photons inelastically off matter. It is a photon-in photon-out spectroscopy for which one can, in principle, measure the energy, momentum, and polarization change of the scattered photon. Compared to other scattering techniques, RIXS has number of unique features. It covers a large scattering phase space, is polarization de-

pendent, element and orbital specific, bulk sensitive [27]. The RIXS spectra at the Ir  $L3$  edge in  $\beta$ -Li<sub>2</sub>IrO<sub>3</sub> were measured by Takayama *et al.* [28] as a function of applied hydrostatic pressure. The  $\beta$ -Li<sub>2</sub>IrO<sub>3</sub> undergoes a pressure-induced structural phase transition at  $P_c \sim 4$  GPa with symmetry lowering to the monoclinic  $C2/c$ . The structural phase transition is accompanied by the formation of Ir<sub>2</sub> dimers on the zigzag chains, with an Ir-Ir distance of  $\sim 2.66$  Å, even shorter than that of metallic Ir. The strong dimerization stabilizes the bonding molecular-orbital state, leads to the collapse of the magnetism and opens the energy gap with a concomitant electronic phase transition from a Mott insulator to band insulator [28]. The experimental measurements showed the drastic reconstruction of the RIXS spectra associated with this dimerization [28]. With increasing pressure above  $P_c$  the prominent peak at  $\sim 0.7$  eV is suppressed strongly. The one at 3.5 eV is broadened but remains in the high-pressure phase. There are some changes at 0.5 to 2.0 eV energy interval, and a shoulder-like feature around 2.8 eV emerges. The aim of the present work is to investigate the RIXS spectra in  $\beta$ -Li<sub>2</sub>IrO<sub>3</sub> compound from the first principles and its evolution under pressure-induced structural phase transitions.

The paper is organized as follows. The computational details are presented in Sec. II. Sec. III presents the electronic structure and theoretically calculated RIXS spectra of the  $\beta$ -Li<sub>2</sub>IrO<sub>3</sub> compound compared with the experimental measurements. Finally, the results are summarized in Sec. IV.

## II. COMPUTATIONAL DETAILS

*a. Crystal structure.* The  $\beta$ -Li<sub>2</sub>IrO<sub>3</sub> crystallizes in the orthorhombic space group  $Fddd$ , with zigzag chains running in alternating directions (see Fig. 1 in Ref. [29] as well as Fig. 1 in Ref. [28]). In the language of the Kitaev interactions, these chains form the  $x$ - and  $y$ -bonds, while the  $z$ -bonds link together adjacent layers of chains. In the hyperhoneycomb Ir sublattice of  $\beta$ -Li<sub>2</sub>IrO<sub>3</sub>, the zigzag Ir chains are connected by the bridging bonds parallel to the  $c$  axis, all the angles between the three Ir-Ir bonds are close to  $120^\circ$ , and the distances between Ir atoms are almost equal (only  $\sim 0.2\%$  difference). At ambient pressure, Ir-Ir bonds along zig-zag chains have a length  $d_{x,y} = 2.9729$  Å, and bonds between the chains  $d_z = 2.9784$  Å.

As pressure increases from ambient pressure to 3.08 GPa, the  $d_{x,y}$  Ir-Ir bonds shrink from 2.9729 to 2.9246 Å; the corresponding  $d_z$  Ir-Ir bonds also decrease from 2.9784 to 2.9379 Å [28, 30]. At  $P_c$ , the bonds between the chains  $d_z$  slightly increase to 3.0129 Å; one of the  $x/y$  bonds also increases to 3.0143 Å, while the other one decreases strongly to 2.6609 Å. Note that this distance is even smaller than the Ir-Ir distance of 2.714 Å in Ir metal. Such a remarkably small interatomic distance strongly suggests the formation of Ir<sub>2</sub> dimers at  $P_c$

[28]. The pressure dependence of the structural parameters of the orthorhombic  $\beta$ -Li<sub>2</sub>IrO<sub>3</sub> can be found in Refs. [28, 30].

*b. Resonant inelastic x-ray scattering.* In the direct RIXS process [27] an incoming photon with energy  $\hbar\omega_{\mathbf{k}}$ , momentum  $\hbar\mathbf{k}$  and polarization  $\epsilon$  excites the solid from a ground state  $|g\rangle$  with energy  $E_g$  to the intermediate state  $|I\rangle$  with energy  $E_I$ . During relaxation the outgoing photon with energy  $\hbar\omega_{\mathbf{k}'}$ , momentum  $\hbar\mathbf{k}'$  and polarization  $\epsilon'$  is emitted, and the solid is in the state  $|f\rangle$  with energy  $E_f$ . As a result an excitation with energy  $\hbar\omega = \hbar\omega_{\mathbf{k}} - \hbar\omega_{\mathbf{k}'}$  and momentum  $\hbar\mathbf{q} = \hbar\mathbf{k} - \hbar\mathbf{k}'$  is created. Our implementation of the code for calculation of the RIXS intensity uses Dirac four-component basis functions [31] in the perturbative approach [32]. RIXS is the second-order process, and its intensity is given by

$$I(\omega, \mathbf{k}, \mathbf{k}', \epsilon, \epsilon') \propto \sum_f \left| \sum_I \frac{\langle f | \hat{H}'_{\mathbf{k}'\epsilon'} | I \rangle \langle I | \hat{H}'_{\mathbf{k}\epsilon} | g \rangle}{E_g - E_I} \right|^2 \times \delta(E_f - E_g - \hbar\omega), \quad (1)$$

where the delta function enforces energy conservation, and the RIXS perturbation operator in the dipolar approximation is given by the lattice sum  $\hat{H}'_{\mathbf{k}\epsilon} = \sum_{\mathbf{R}} \hat{\alpha}\epsilon \exp(-i\mathbf{k}\mathbf{R})$ , where  $\hat{\alpha}$  are Dirac matrices. Both  $|g\rangle$  and  $|f\rangle$  states are dispersive so the sum over final states is calculated using the linear tetrahedron method [33].

Detailed expressions for the matrix elements in the electric dipole approximation in the framework of fully relativistic Dirac representation were presented in Ref. [34].

*c. Calculation details* The details of the computational method are described in our previous papers [35–38] and here we only mention several aspects. Band structure calculations were performed using the fully relativistic linear muffin-tin orbital (LMTO) method [39, 40]. This implementation of the LMTO method uses four-component basis functions constructed by solving the Dirac equation inside an atomic sphere [31]. The exchange-correlation functional of a GGA-type was used in the version of Perdew, Burke and Ernzerhof (PBE) [41]. Brillouin zone (BZ) integration was performed using the improved tetrahedron method [42]. The basis consisted of Ir  $s$ ,  $p$ ,  $d$ , and  $f$ ; and Li and O  $s$ ,  $p$ , and  $d$  LMTO's.

To take into account electron-electron correlation effects, we used in this work the "relativistic" generalization of the rotationally invariant version of the LSDA+ $U$  method [43] which takes into account SO coupling so that the occupation matrix of localized electrons becomes non-diagonal in spin indexes. We use in our calculations the value of  $U_{\text{eff}} = 1.5$  eV ( $U = 2.15$  eV and  $J_H = 0.65$  eV) which gives the best agreement between the calculated and experimental optical spectra in the  $\beta$ -Li<sub>2</sub>IrO<sub>3</sub> [29].

We used in our calculations vector  $\mathbf{q} = (0, 10, 0)$ . Takayama *et al.* [28] show that at a low pressure of 0.9

GPa, the RIXS spectrum at the Ir  $L3$  for the single crystal agrees well with that of the polycrystalline sample at ambient pressure. This supports the idea that the  $d-d$  excitations show only a small  $\mathbf{q}$  dependence in  $\beta$ - $\text{Li}_2\text{IrO}_3$ .

### III. ELECTRONIC STRUCTURE

Figure 1 presents the *ab initio* energy band structure of the  $\beta$ - $\text{Li}_2\text{IrO}_3$  in the energy range of  $-3$  to  $5$  eV for the ambient pressure  $Fddd$  phase, calculated in the fully relativistic Dirac GGA+SO approximation (the upper panel) and with taking into account Coulomb correlations in the GGA+SO+ $U$  approximation (middle panel). The lower panel presents the energy band structure of the  $\beta$ - $\text{Li}_2\text{IrO}_3$  for the high-pressure phase ( $C2/c$ ) in the GGA+SO approach.

In  $\text{Li}_2\text{IrO}_3$  each  $\text{Ir}^{4+}$  ion surrounded by six  $\text{O}^{2-}$  ions has five valent  $5d$  electrons. The octahedral crystal field largely splits the Ir  $t_{2g}$  and  $e_g$  manifolds, so that all five electrons occupy the  $t_{2g}$  manifold. As a result of strong SO coupling ( $\Delta_{SO} \sim 0.78$  eV), the six  $t_{2g}$  orbitals are further separated into two manifolds with  $J_{\text{eff}} = 3/2$  and  $J_{\text{eff}} = 1/2$  [Fig. 1(a)]. The  $J_{\text{eff}} = 3/2$  states are fully filled and the  $J_{\text{eff}} = 1/2$  states are half filled. The functions of the  $J_{\text{eff}} = 3/2$  quartet are dominated by  $d_{3/2}$  states with some minor influence of  $d_{5/2}$  states, which is determined by the relative strengths of SO coupling and crystal-field splitting. The  $J_{\text{eff}} = 1/2$  functions, on the other hand, are given by linear combinations of  $d_{5/2}$  states only. This allows one to identify bands with pure  $d_{5/2}$  character as originating from  $J_{\text{eff}} = 1/2$  states.

The GGA+SO approximation produces a metallic ground state in the  $\beta$ - $\text{Li}_2\text{IrO}_3$  [Fig. 1(a)], in contradiction with resistivity measurements which claim that the  $\beta$ - $\text{Li}_2\text{IrO}_3$  is a Mott insulator. To produce the correct ground state we have to take into account Hubbard electron-electron correlations. The  $J_{\text{eff}} = 1/2$  spin-orbit integrated states form a narrow band so that even small  $U_{\text{eff}}=1.5$  eV opens Mott gap and splits the  $5d_{5/2}$  ( $J_{\text{eff}} = 1/2$ ) band into the upper Hubbard band (UHB) above the Fermi level [red lines in Fig. 1(b)] and lower Hubbard band (LHB) below the Fermi level [magenta lines in Fig. 1(b)]. The formation of the  $J_{\text{eff}}$  bands is a natural consequence of the  $J_{\text{eff}}$  Hubbard model. The  $e_g$  orbitals are almost degenerate at ambient pressure occupying the 3.4–4.2 eV energy interval.

The  $\beta$ - $\text{Li}_2\text{IrO}_3$  compound shows strong SO coupling concurrent with electronic correlations, leading to interesting electronic and magnetic properties. Due to a delicate balance between these interactions, minor changes in its parameters may result in a drastic alteration of the magnetic ground state. These changes may deviate from long-range magnetic order and perhaps lead towards unexplored phases such as a quantum spin liquid. One of the experimental approaches suited to achieving this goal is the application of an external hydrostatic pressure. The application of external pressure is a very efficient

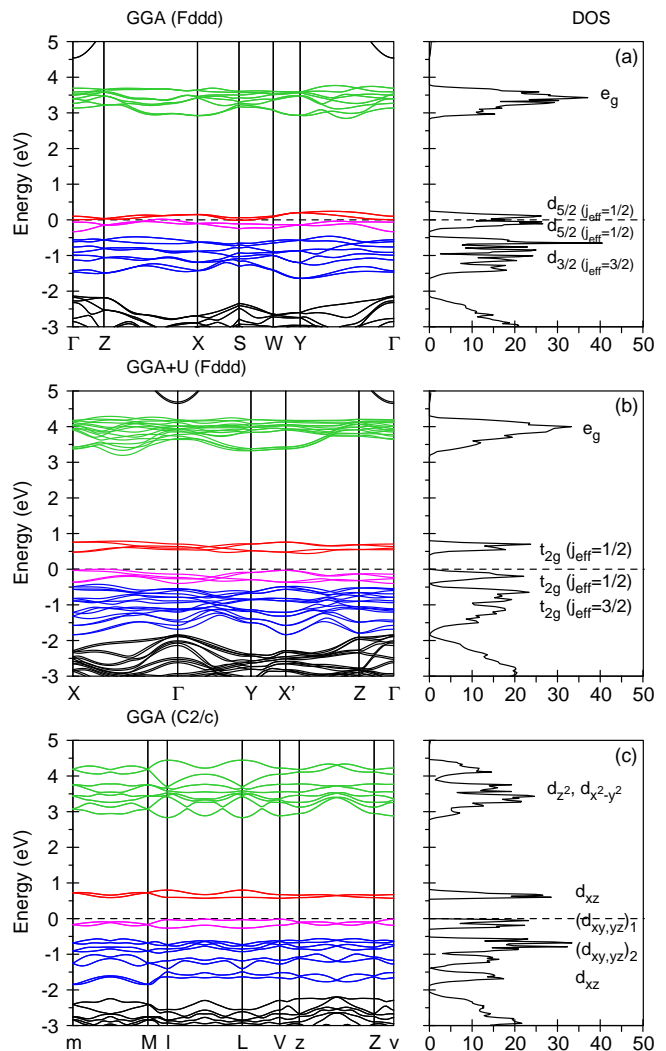


FIG. 1: (Color online) (a) The *ab initio* energy band structure of the  $\beta$ - $\text{Li}_2\text{IrO}_3$  for the ambient pressure phase ( $Fddd$ ) in the fully relativistic Dirac GGA+SO approximation; (b) the energy band structure of the  $\beta$ - $\text{Li}_2\text{IrO}_3$  for the ambient pressure phase ( $Fddd$ ) in the GGA+SO+ $U$  approximation; (c) the energy band structure of the  $\beta$ - $\text{Li}_2\text{IrO}_3$  for the high-pressure phase ( $C2/c$ ) in the GGA+SO approach.

and clean way to adjust the ground state of materials without introducing additional scattering centers. Hydrostatic pressure was applied to the hyperhoneycomb material,  $\beta$ - $\text{Li}_2\text{IrO}_3$ , and it was found that the crystal structure of the  $\beta$ - $\text{Li}_2\text{IrO}_3$  is transformed from the orthorhombic  $Fddd$  symmetry to the monoclinic  $C2/c$  one at  $P_c \sim 4$  GPa [28, 30]. Pressure reduces the tendency toward magnetism, thus diminishing the energetic advantage of forming an antiferromagnetic state, and it brings Ir ions closer together, enhancing the advantage of forming covalent bonds. The structural  $Fddd \rightarrow C2/c$  phase transition at  $P_c \sim 4$  GPa is accompanied by a magnetic collapse, and spin and orbital magnetic moments at the Ir site vanish abruptly [29].

Figure 1(c) presents the *ab initio* energy band structure of the  $\beta$ -Li<sub>2</sub>IrO<sub>3</sub> for monoclinic  $C2/c$  structure calculated in fully relativistic Dirac GGA+SO approximation. The calculations reveal that a pressure-induced structural phase transition  $Fddd \rightarrow C2/c$  at  $P_c \sim 4$  GPa is accompanied by the electronic phase transition from magnetic Mott insulator to nonmagnetic (NM) band insulator. The crystal field at the Ir site ( $C1$  point symmetry) causes the splitting of  $5d$  orbitals into five singlets  $z^2$ ,  $x^2 - y^2$ ,  $xy$ ,  $yz$ , and  $xz$ . The electronic structure of the high-pressure  $C2/c$  structure possesses an empty peak in proximity to the Fermi level which almost coincides with the position of the corresponding UHB  $J_{\text{eff}} = 1/2$  states in Mott insulator at ambient pressure. However, these two peaks have completely different nature. The formation of Ir<sub>2</sub> dimers in the hyperhoneycomb lattice at high-pressure gives rise to bonding and antibonding molecular-orbital states [28]. In a new coordinate system ( $x' = (x + z)/\sqrt{2}$ ,  $y' = (x - z)/\sqrt{2}$ ,  $z' = y$ ) with  $d_{xz}$  orbital, directed along the dimer  $Y$  bond the two subbands with predominant  $d_{xz}$  character can be seen in Fig. 1(c) at 0.7 eV above the Fermi level and at  $-1.7$  eV below the Fermi level. They can be assigned to the antibonding and the bonding states of Ir<sub>2</sub> dimer molecules. The large bonding-antibonding splitting stabilizes the  $d_{xz}$ -orbital-dominant anti-bonding state of  $t_{2g}$  holes and makes the system a NM band insulator. The remaining  $d_{xy}$  and  $d_{yz}$  orbitals are very strongly mixed by SO coupling and cannot be separated from each other, therefore we would call them  $d_{xy}/d_{yz}$  orbitals. These orbitals contribute to the subbands between the  $d_{xz}$ -bonding and -antibonding subbands due to weaker hybridization between the nearest-neighbor Ir atoms than that of  $d_{xy}/d_{yz}$  orbitals. An energy gap is formed between the mixed  $d_{xy}/d_{yz}$  subbands and the empty antibonding  $d_{xz}$  subband. SO coupling separates the  $d_{xy}/d_{yz}$  bands into two groups  $(d_{xy}/d_{yz})_1$  and  $(d_{xy}/d_{yz})_2$  situated at 0 to  $-0.3$  eV and  $-0.5$  to  $-1.4$  eV, respectively.

Due to the strong distortion of IrO<sub>6</sub> octahedra in the  $C2/c$  high-pressure phase the  $e_g$  orbitals, which are almost degenerate at ambient pressure, split to  $z^2$  and  $x^2 - y^2$  states and become broader occupying the 3–4.5 eV energy interval.

#### IV. Ir $L_3$ RIXS SPECTRUM

Figure 2 presents the experimentally measured RIXS spectrum at the Ir  $L_3$  edge for the  $\beta$ -Li<sub>2</sub>IrO<sub>3</sub> for the ambient pressure [28] (green open circles) compared with the theoretically calculated ones in the GGA+SO (the upper panel) and GGA+SO+ $U$  approximations (middle panel) for the  $Fddd$  phase. The lower panel shows the experimental RIXS spectrum for high-pressure phase ( $C2/c$ ) above  $P_c$  [28] (open magenta circles) compared with the theoretically calculated spectra in the GGA+SO approximation.

The experimental RIXS spectrum at the Ir  $L_3$  edge for

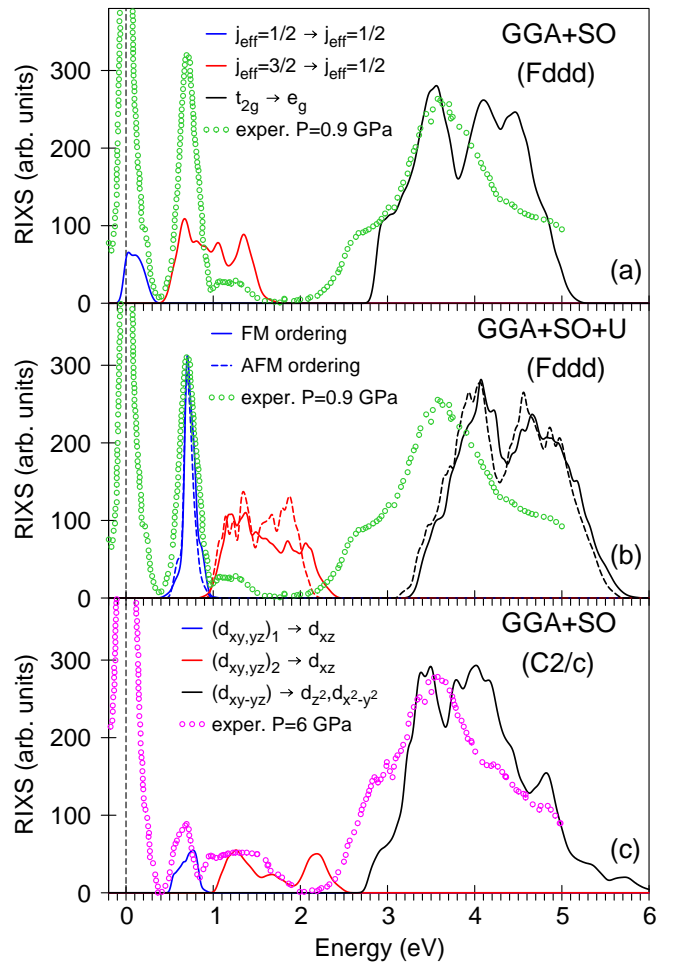


FIG. 2: (Color online) (a) The experimental RIXS spectra at the Ir  $L_3$  edge for the  $\beta$ -Li<sub>2</sub>IrO<sub>3</sub> for the ambient pressure at room temperature [28] (open green circles) compared with the theoretically calculated spectra in the GGA+SO approximation; (b) the experimental RIXS spectra at the Ir  $L_3$  edge for the  $\beta$ -Li<sub>2</sub>IrO<sub>3</sub> for the ambient pressure [28] (open green circles) compared with the theoretically calculated spectra in the GGA+SO+ $U$  approach for the FM ordering along the  $c$  direction (full curves) and for the AFM ordering along the  $c$  direction (dashed curves); (c) The experimental RIXS spectra at the Ir  $L_3$  edge for the  $\beta$ -Li<sub>2</sub>IrO<sub>3</sub> for high-pressure phase ( $C2/c$ ) above  $P_c$  [28] (open magenta circles) compared with the theoretically calculated spectra in the GGA+SO approximation.

the ambient pressure in addition to the elastic scattering peak at 0 eV, possesses a sharp narrow peak at around 0.7 eV, followed by a broad structure between 1 eV and 2 eV, and a broad peak centered at around 3.5 eV. The latter represents the excitations from Ir  $5d$   $t_{2g}$  to  $e_g$  manifolds. The peak at  $\sim 0.7$  eV can be assigned to the local excitation between the filled  $J_{\text{eff}} = 1/2$  and the empty  $J_{\text{eff}} = 1/2$  states. The fine structure at 1 eV to 2 eV is derived by the excitation between the filled  $J_{\text{eff}} = 3/2$  and the empty  $J_{\text{eff}} = 1/2$  states.

The GGA+SO approximation fails to reproduce a sharp narrow peak at around 0.7 eV. The corresponding peak is situated at 0.1 eV [blue curve in Fig. 2(a)] and has much smaller intensity in comparison with the experimentally observed peak at 0.7 eV. On the other hand, the theory correctly reproduces the energy position of the wide peak at 3.5 eV responsible for the  $t_{2g} \rightarrow e_g$  transitions [black curve in Fig. 2(a)]. In contrast, the GGA+SO+ $U$  approach well describes the shape and intensity of the LHB  $J_{\text{eff}} = 1/2 \rightarrow$  UHB  $J_{\text{eff}} = 1/2$  peak, however, it overestimates the intensity of  $J_{\text{eff}} = 3/2 \rightarrow J_{\text{eff}} = 1/2$  transitions presented by the red curve in Fig. 2(b). In addition, the theoretically calculated excitations from Ir  $5d$   $t_{2g}$  to  $e_g$  manifolds are shifted towards higher energies by approximately 0.7 eV in comparison with the experiment. We calculated the RIXS spectra for the ferromagnetic (FM) and antiferromagnetic (AFM) ordering along the  $c$  direction and in the  $ab$  plane for the  $Fddd$  phase and found that the type of magnetic ordering weakly influences on the shape and intensity of the major fine structures of Ir  $L_3$  RIXS spectrum, especially low energy peak at 0.7 eV [Fig. 2(b)].

Due to applying of the Hubbard  $U$ , Ir  $5d$  occupied states are shifted downward by  $U_{\text{eff}}/2$  and the empty  $d$  states are shifted upward by this amount relative to the Fermi energy. The Coulomb repulsion splits the half-filled  $J_{\text{eff}} = 1/2$  band into an empty UHB and occupied LHB, open the energy gap and place the UHB at 0.7 eV above the Fermi level in good agreement with the optical [29] and RIXS measurements [28]. Because we apply the Hubbard  $U$  to all the Ir  $5d$  states, it also shifts the empty  $t_{2g}$  states upward by  $U_{\text{eff}}/2$  and places them at higher energy than it detected in the RIXS experiment. It looks like the correlation effects are mostly important for the  $5d$  states in close vicinity of the Fermi level. The position of the  $e_g$  states are correctly reproduced by the GGA+SO approximation without taking into account the electron correlations [see Fig. 2(a)].

Both the ambient pressure ( $Fddd$ ) and the high-pressure ( $C2/c$ ) phases possess an empty peak in proximity to the Fermi level at around 0.7 eV (Fig. 1), therefore one would expect similar RIXS spectra at the low energy range below 1 eV. However, RIXS measurements show the drastic reconstruction of the electronic structure associated with the Ir dimerization [28]. The 0.7 eV peak is suppressed strongly in the high-pressure dimerized phase above 4 GPa. There are some changes also at 1 to 2 eV energy interval. The wide peak at 3.5 eV associated with the excitations from Ir  $5d$   $t_{2g}$  to  $e_g$  manifolds is broadened. The latter is due to the strong distortion of the  $\text{IrO}_6$  octahedra in the  $C2/c$  high-pressure phase: the  $e_g$  orbitals which are almost degenerated at ambient pressure split to  $z^2$  and  $x^2 - y^2$  states and became broader. The GGA+SO approximation relatively well reproduces all the fine structures of the RIXS spectrum under the pressure above the  $P_c$  [see Fig. 2(c)]. The question is why the prominent peak at 0.7 eV is strongly suppressed in the RIXS spectra in the high-pressure  $C2/c$  phase.

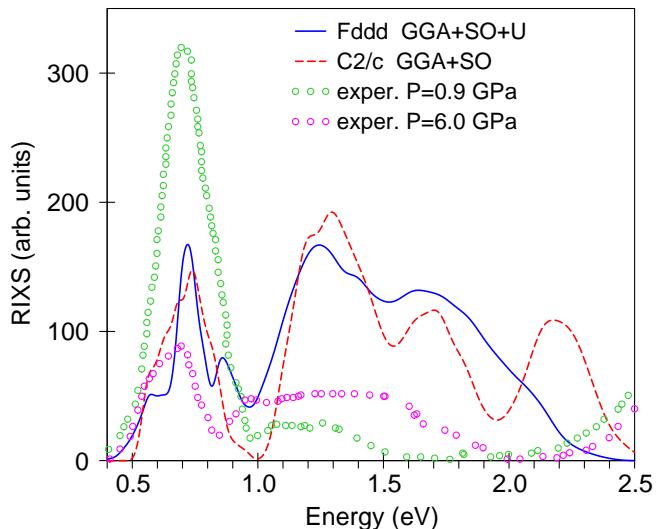


FIG. 3: (Color online) The comparison of RIXS spectra for the ambient (green circles) and high-pressure above  $P_c$  (magenta circles) phases [28] with the constant matrix elements (JDOS) calculated for the ambient pressure phase ( $Fddd$ ) in the GGA+SO+ $U$  approximation (full blue curve) and for the high-pressure phase ( $C2/c$ ) in the GGA+SO approach (dashed red curve).

The pressure-induced structural phase transition at  $P_c \sim 4$  GPa is accompanied by slight decrease of width of the  $d_{xz}$  antibonding empty states at 0.7 eV in comparison with the empty UHB ( $J_{\text{eff}} = 1/2$ ) states in the  $Fddd$  phase (see Fig. 8 in Ref. [29]). Therefore, one would expect more narrow RIXS peak at 0.7 eV in the high-pressure phase and, at least, the similar intensity in comparison with the  $Fddd$  phase.

The RIXS spectrum is a convolution of the densities of the occupied and empty valence states [so called joint density of states (JDOS)], weighted by appropriate matrix elements. Fig. 3 presents comparison of the experimentally measured RIXS spectra for the ambient and high-pressure phases [28] with the JDOS calculated for the ambient pressure phase ( $Fddd$ ) in the GGA+SO+ $U$  approximation (the full blue curve) and for the high-pressure phase ( $C2/c$ ) in the GGA+SO approach (the dashed red curve). We see that without taking into account the corresponding matrix elements the theoretically calculated prominent peak at 0.7 eV has similar intensity for both the phases and significantly differ from the experimentally measured ones. Therefore, the reason of strong suppression of this peak in high-pressure phase is the significantly different matrix elements in these two phases.

There are two reasons why the matrix elements can be strongly altered in the phase transition at the  $P_c$ . First, the prominent peak at 0.7 eV above the Fermi level is created by different orbitals ( $t_{2g}$  states in  $Fddd$  phase and almost pure  $d_{xz}$  orbitals in high-pressure  $C2/c$  phase). Yang *et al.* [44] showed that angular matrix elements for

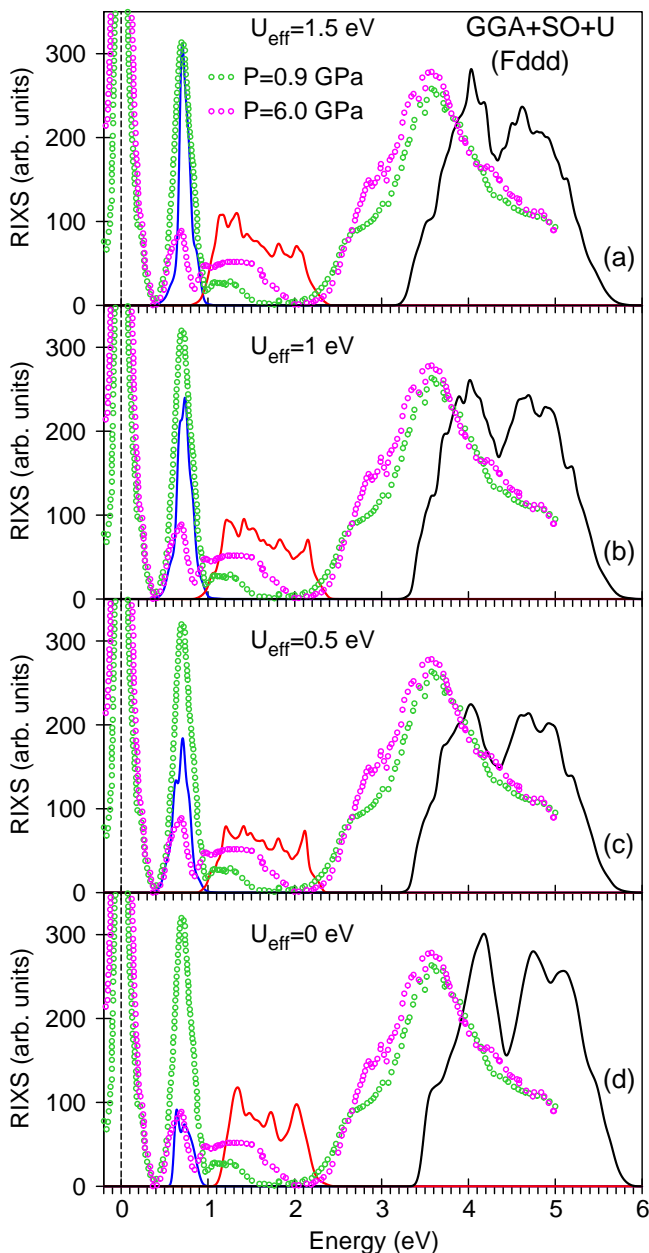


FIG. 4: (Color online) The experimental RIXS spectra at the Ir  $L_3$  edge for the  $\beta$ - $\text{Li}_2\text{IrO}_3$  for the ambient pressure ( $Fddd$ ) (open green circles) and high-pressure (open magenta circles) ( $C2/c$ ) phases above  $P_c$  [28] compared with the theoretically calculated spectra in the GGA+SO+ $U$  approximation for different values of  $U_{\text{eff}}$  at the Ir site.

dipole allowed transitions in x-ray absorption at the  $L_3$  edge strongly depend on the type of the orbitals involved in the transitions. Second, the matrix elements can be strongly modified due to different ground states of the phases: a magnetic strongly correlated Mott insulator at ambient pressure and a NM band insulator at  $P_c$  with vanished Hubbard  $U$ .

At ambient pressure,  $\beta$ - $\text{Li}_2\text{IrO}_3$  shows a rather highly

symmetric honeycomb structure with a bond disproportionation of less than 0.2%. If pressure is increased from ambient pressure Ir-Ir bonds monotonically shrink under the pressure and at the structural  $Fddd \rightarrow C2/c$  phase transition at  $P_c = 4.4$  GPa one of the  $x/y$  bonds is strongly decreased to 2.6609 Å [30], which is even smaller than the Ir-Ir distance of 2.714 Å in Ir metal. Such the dimerization enhances the advantage of forming covalent bonds which is accompanied by a magnetic collapse, spin and orbital magnetic moments at the Ir site are vanished abruptly [29]. Pressure reduces Coulomb correlation Hubbard parameter  $U_{\text{eff}}$  which decreases from 1.5 eV for ambient pressure to zero at  $P_c = 4.4$  GPa [29] and reduces also the effective SO interaction at Ir site. It is supported experimentally by the corresponding pressure dependence of the branching ratio  $\text{BR} = I_{L_3}/I_{L_2}$ , where  $I_{L_{2,3}}$  is the integrated intensity of the isotropic x-ray absorption spectra at the  $L_{2,3}$  edges [30].

We examine the dependence of the RIXS spectra on the Hubbard  $U$  at the Ir site calculating the spectra for  $U=2.15$  eV, 1.9 eV, 1.65 eV, 1.4 eV, 1.15 eV, 0.9 eV, and 0.65 eV. It corresponds to  $U_{\text{eff}}=1.5$  eV, 1.25 eV, 1.0 eV, 0.75 eV, 0.5 eV, 0.25 eV, and 0 eV. The results of such calculations for the RIXS spectra dependence on the  $U_{\text{eff}}$  are shown in Fig. 4. The reduction of the  $U_{\text{eff}}$  leads to gradually reduction of the peak intensity of the prominent peak at 0.7 eV. For  $U_{\text{eff}}=0$  eV this peak reduces to the value observed in the high-pressure phase. We found that the energy gap is also reduced by 0.102 eV, 0.202 eV and 0.301 eV for  $U_{\text{eff}} = 1.25$  eV, 1.0, and 0.75 eV, respectively. The gap is closed for  $U_{\text{eff}} = 0.5$  eV. As a result, the prominent peak situated at 0.7 eV shifts towards smaller energy with decreasing of the  $U_{\text{eff}}$  parameter. To show more clearly how the peak intensity at 0.7 eV depends on the  $U_{\text{eff}}$  we keep this peak artificially at 0.7 eV above the Fermi level in Fig. 4.

We can conclude that the drastic reconstruction of the RIXS spectrum associated with the structural  $Fddd \rightarrow C2/c$  phase transition at  $P_c$  can be related to the Coulomb correlations disappearing in the high-pressure  $C2/c$  phase.

## V. CONCLUSIONS

The electronic structure and RIXS spectra of the hyperhoneycomb iridate  $\beta$ - $\text{Li}_2\text{IrO}_3$  were investigated theoretically within the DFT-GGA approach in the framework of the fully relativistic spin-polarized Dirac LMTO band-structure method, taking into account Coulomb electron-electron correlations.

The GGA+SO approximation produces a metallic ground state in the  $\beta$ - $\text{Li}_2\text{IrO}_3$ , in contradiction with resistivity measurements which claims that the  $\beta$ - $\text{Li}_2\text{IrO}_3$  is a spin-orbit Mott insulator. To produce the correct ground state we have to take into account Hubbard electron-electron correlations. The Coulomb repulsion  $U$  splits the half-filled  $J_{\text{eff}} = 1/2$  band into an empty upper Hubbard

band with pure  $d_{5/2}$  character well separated from the lower  $J_{\text{eff}} = 1/2$  Hubbard band and the  $J_{\text{eff}} = 3/2$  states below the Fermi level. We found that the GGA+SO+ $U$  approach with Hubbard  $U_{\text{eff}} = 1.5$  eV well describes the RIXS spectrum at the Ir  $L_3$  edge for ambient pressure in the  $Fddd$  phase.

The hyperhoneycomb iridate  $\beta\text{-Li}_2\text{IrO}_3$ , a spin-orbit Mott insulator, is on the border of the magnetic ordering with relatively weak Coulomb electron-electron correlations ( $U_{\text{eff}} = 1.5$  eV). The  $\beta\text{-Li}_2\text{IrO}_3$  undergoes a pressure-induced structural and magnetic phase transitions at  $P_c \sim 4$  GPa with symmetry lowering to the monoclinic  $C2/c$ . The structural phase transition is accompanied by a dimerization of the previously equally long  $x/y$  Ir-Ir bonds. We found remarkable NM ground states of the  $\beta\text{-Li}_2\text{IrO}_3$  at  $P_c$ , with a concomitant electronic phase transition from a Mott insulator to band insulators.

The energy band structure of the  $\beta\text{-Li}_2\text{IrO}_3$  for the ambient pressure phase ( $Fddd$ ) in the GGA+SO+ $U$  approximation and for the high-pressure phase ( $C2/c$ ) possess similar peaks in the DOSs with the same energy positions. However, these peaks have completely different nature. There are empty UHB ( $J_{\text{eff}} = 1/2$ ) and occupied LHB ( $J_{\text{eff}} = 1/2$ ) peaks at  $\sim 0.7$  eV and  $-0.2$  eV, respectively, in the  $Fddd$  phase. The similar peaks in high-pressure  $C2/c$  phase are assigned to the  $d_{xz}$  antibonding

states of  $\text{Ir}_2$  dimer molecules (at 0.7 eV) and mixture of the  $(d_{xy} - d_{yz})_1$  states. The peaks between  $-0.5$  eV and  $-1.9$  eV belong to the  $J_{\text{eff}} = 3/2$  states in  $Fddd$  phase and the  $(d_{xy} - d_{yz})_2$  states plus the  $d_{xz}$  molecular bonding states in the high-pressure  $C2/c$  phase.

The drastic reconstruction of the RIXS spectral peak at 0.7 eV associated with the structural  $Fddd \rightarrow C2/c$  phase transition at  $P_c$  can be related to disappearing of the Coulomb correlations.

### Acknowledgments

We are thankful to Dr. Alexander Yaresko from Max-Planck-Institute FKF in Stuttgart for very long and helpful discussions. V.N.A. gratefully acknowledges the hospitality at the University of Bialystok during his stay there. D.A.K. gratefully acknowledges the hospitality at the Max-Planck-Institute FKF during his stay in Stuttgart.

The studies were supported by the National Academy of Sciences of Ukraine within the budget program KP-KBK 6541230-3A "Support for the development of priority areas of scientific research".

- 
- [1] G. Jackeli and G. Khaliullin, Phys. Rev. Lett. **102**, 017205 (2009).
  - [2] W. Witczak-Krempa, G. Chen, Y. B. Kim, and L. Balents, Ann. Rev. Condens. Matter Phys. **89**, 025003 (2014).
  - [3] I. Kimchi, J. G. Analytis, and A. Vishwanath, Phys. Rev. B **90**, 205126 (2014).
  - [4] A. Kitaev, Ann. Phys. **321**, 2 (2006).
  - [5] S. M. Albrecht, A. P. Higginbotham, M. Madsen, F. Kuemmeth, T. S. Jespersen, J. Nygrd, P. Krogstrup, and C. M. Marcus, Nature **531**, 206 (2016).
  - [6] S. M. Winter, A. A. Tsirlin, M. Daghofer, J. van den Brink, Y. Singh, P. Gegenwart, and R. Valentini, J. Phys.: Condens. Matter **29**, 493002 (2017).
  - [7] R. Schaffer, E. K.-H. Lee, B.-J. Yang, and Y. B. Kim, Rep. Prog. Phys. **79**, 094504 (2016).
  - [8] F. Ye, S. Chi, H. Cao, B. C. Chakoumakos, J. A. Fernandez-Baca, R. Custelcean, T. F. Qi, O. B. Korneta, and G. Cao, Phys. Rev. B **85**, 180403 (2012).
  - [9] A. Shitade, H. Katsura, J. Kunes, X.-L. Qi, S.-C. Zhang, and N. Nagaosa, Phys. Rev. Lett. **102**, 256403 (2009).
  - [10] M. Z. Hasan and C. L. Kane, Rev. Mod. Phys. **82**, 3045 (2010).
  - [11] J. Chaloupka, G. Jackeli, and G. Khaliullin, Phys. Rev. Lett. **110**, 097204 (2013).
  - [12] G. Cao, T. F. Qi, L. Li, J. Terzic, V. S. Cao, S. J. Yuan, M. Tovar, G. Murthy, and R. K. Kaul, Phys. Rev. B **88**, 220414 (2013).
  - [13] A. Biffin, R. D. Johnson, S. Choi, F. Freund, S. Manni, A. Bombardi, P. Manuel, P. Gegenwart, and R. Coldea, Phys. Rev. B **90**, 205116 (2014).
  - [14] J. Knolle, G.-W. Chern, D. L. Kovrizhin, R. Moessner, and N. B. Perkins, Phys. Rev. Lett. **113**, 187201 (2014).
  - [15] T. Takayama, A. Kato, R. Dinnebier, J. Nuss, H. Kono, L. S. I. Veiga, G. Fabbris, D. Haskel, and H. Takagi, Phys. Rev. Lett. **114**, 077202 (2015).
  - [16] R. Schaffer, E. K.-H. Lee, Y.-M. Lu, and Y. B. Kim, Phys. Rev. Lett. **114**, 116803 (2015).
  - [17] A. Glamazda, P. Lemmens, S. H. Do, Y. S. Choi, and K. Y. Choi, Nat. Commun. **7**, 12286 (2016).
  - [18] B. J. Kim, H. Jin, S. J. Moon, J.-Y. Kim, B.-G. Park, C. S. Leem, J. Yu, T. W. Noh, C. Kim, S.-J. Oh, et al., Phys. Rev. Lett. **101**, 076402 (2008).
  - [19] H.-S. Kim, Y. B. Kim, and H.-Y. Kee, Phys. Rev. B **94**, 245127 (2016).
  - [20] E. K.-H. Lee and Y. B. Kim, Phys. Rev. B **91**, 064407 (2015).
  - [21] I. Kimchi, R. Coldea, and A. Vishwanath, Phys. Rev. B **91**, 245134 (2015).
  - [22] V. M. Katukuri, R. Yadav, L. Hozoi, S. Nishimoto, and J. van den Brink, Sci. Rep. **6**, 29585 (2016).
  - [23] A. Ruiz, A. Frano, N. P. Breznay, I. Kimchi, T. Helm, I. Oswald, J. Y. Chan, R. Birgeneau, Z. Islam, and J. G. Analytis, Nature Comm. **8**, 961 (2017).
  - [24] S. Ducatman, I. Rousochatzakis, and N. B. Perkins, Phys. Rev. B **97**, 125125 (2018).
  - [25] M. Majumder, R. S. Manna, G. Simutis, J. C. Orain, T. Dey, F. Freund, A. Jesche, R. Khasanov, P. K. Biswas, E. Bykova, et al., Phys. Rev. Lett. **120**, 237202 (2018).
  - [26] V. Hermann, M. Altmeyer, J. Ebad-Allah, F. Freund, A. Jesche, A. A. Tsirlin, M. Hanfland, P. Gegenwart, I. I. Mazin, D. I. Khomskii, et al., Phys. Rev. B **97**,

- 020104(R) (2018).
- [27] L. J. P. Ament, M. van Veenendaal, T. P. Devereaux, J. P. Hill, and J. van den Brink, *Rev. Mod. Phys.* **83**, 705 (2011).
- [28] T. Takayama, A. Krajewska, A. S. Gibbs, A. N. Yaresko, H. Ishii, H. Yamaoka, K. Ishii, N. Hiraoka, N. P. Funnell, C. L. Bull, et al., *Phys. Rev. B* **99**, 125127 (2019).
- [29] V. N. Antonov, S. Uba, and L. Uba, *Phys. Rev. B* **98**, 245113 (2018).
- [30] L. S. I. Veiga, M. Etter, K. Glazyrin, F. Sun, J. C. A. Escanhoela, G. Fabbri, J. R. L. Mardegan, P. S. Malavi, Y. Deng, P. P. Stavropoulos, et al., *Phys. Rev. B* **96**, 140402(R) (2017).
- [31] V. V. Nemoshkalenko, A. E. Krasovskii, V. N. Antonov, V. N. Antonov, U. Fleck, H. Wonn, and P. Ziesche, *Phys. status solidi B* **120**, 283 (1983).
- [32] E. Arola, P. Strange, and B. L. Gyorffy, *Phys. Rev. B* **55**, 472 (1997).
- [33] G. Lehmann and M. Taut, *Phys. status solidi B* **54**, 469 (1972).
- [34] D. A. Kukusta and A. N. Yaresko, in *Resonant inelastic x-ray scattering spectra from band structure calculations* (Workshop "Strongly Correlated Electron Systems", Ringberg Castle, Germany, 2018, unpublished).
- [35] V. N. Antonov, O. Jepsen, A. N. Yaresko, and A. P. Shpak, *J. Appl. Phys.* **100**, 043711 (2006).
- [36] V. N. Antonov, B. N. Harmon, A. N. Yaresko, and A. P. Shpak, *Phys. Rev. B* **75**, 184422 (2007).
- [37] V. N. Antonov, A. N. Yaresko, and O. Jepsen, *Phys. Rev. B* **81**, 075209 (2010).
- [38] V. N. Antonov, D. A. Kukusta, and L. V. Bekenov, *Phys. Rev. B* **102**, 195134 (2020).
- [39] O. K. Andersen, *Phys. Rev. B* **12**, 3060 (1975).
- [40] A. Y. Perlov, A. N. Yaresko, and V. N. Antonov, PY-LMTO, A Spin-polarized Relativistic Linear Muffin-tin Orbitals Package for Electronic Structure Calculations (1995, unpublished).
- [41] J. P. Perdew, K. Burke, and M. Ernzerhof, *Phys. Rev. Lett.* **77**, 3865 (1996).
- [42] P. E. Blöchl, O. Jepsen, and O. K. Andersen, *Phys. Rev. B* **49**, 16223 (1994).
- [43] A. N. Yaresko, V. N. Antonov, and P. Fulde, *Phys. Rev. B* **67**, 155103 (2003).
- [44] X. Yang, A. N. Yaresko, V. N. Antonov, and O. K. Andersen, preprint cond-mat/0911.4349v (2009).